The ROYAL COLLEGE *of* OPHTHALMOLOGISTS

ARTICLE

Check for updates

Near infrared autofluorescence imaging of retinal pigmented epithelial cells using 663 nm excitation

Kari V. Vienola [1,4 ✉], Min Zhang[1], Valerie C. Snyder[1], Kunal K. Dansingani [1], José-Alain Sahel[1] and Ethan A. Rossi[1,2,3]

PURPOSE: Fundus autofluorescence (AF) using adaptive optics scanning laser ophthalmoscopy (AOSLO) enables morphometric analysis of individual retinal pigmented epithelial (RPE) cells. However, only a few excitation wavelengths in the visible and near-infrared have been evaluated. Visible light excitation (<600 nm) presents additional safety hazards and is uncomfortable for patients. Near-infrared excitation (>700 nm) overcomes those problems but introduces others, including decreased AF signal and cone signatures that obscure RPE structure. Here we investigated the use of an intermediate wavelength, 663 nm, for excitation and compared it to 795 nm.
METHODS: Subjects were imaged using AOSLO equipped with a detection channel to collect AF emission between 814 and 850 nm. Two light sources (663 and 795 nm) were used to excite the retinal fluorophores. We recorded 90 s videos and registered them with custom software to integrate AF images for analysis.
RESULTS: We imaged healthy eyes and an eye with pattern dystrophy. Similar AF microstructures were detected with each excitation source, despite ~4 times lower excitation power with 663 nm. The signal-to-noise values showed no meaningful difference between 663 nm and 795 nm excitation and a similar trend was observed for image contrast between the two excitation wavelengths.
CONCLUSIONS: Lower light levels can be used with shorter wavelength excitation to achieve comparable images of the microstructure of the RPE as have been obtained using higher light levels at longer wavelengths. Further experiments are needed to fully characterize AF across spectrum and determine the optimal excitation and emission bandwidths that balance efficiency, patient comfort, and efficacy.

Eye (2022) 36:1878–1883; https://doi.org/10.1038/s41433-021-01754-0

INTRODUCTION

Fundus autofluorescence (FAF) is a standard tool used in the clinic [1, 2] that provides useful diagnostic information about outer retinal health in diseases such as age-related macular degeneration (AMD) [3, 4]. Typically, FAF is most often carried out using scanning laser ophthalmoscopes with field-of-view (FOV) varying from 30 to 200°. Though these systems are robust and provide a wide area of coverage, they lack the sensitivity and resolution to detect microscopic alterations and measure the properties of single cells.

Retinal pigment epithelium (RPE) changes at the level of single cells may be a useful biomarker to diagnose diseases at early stages, before the damage extends to photoreceptors and irreversible vision loss occurs. By utilizing the naturally occurring fluorophores in these cells, such as lipofuscin and melanin, visualization of these cells becomes possible [5, 6]. Fundus autofluorescence (FAF) has typically been observed using either short or near infrared wavelengths for fluorophore excitation. Short wavelength autofluorescence (SWAF) is performed with a blue-shifted excitation, commonly 488 nm or 532 nm, with emission detected in the visible (575–700 nm) range. Near infrared

autofluorescence (NIRAF) emission is usually detected from 800 to 900 nm, with excitation wavelengths in the 750–800 nm range.

Near infrared autofluorescence (NIRAF) imaging using adaptive optics (AO-IRAF) is an emerging technology that has received interest due to its relatively straightforward implementation in existing adaptive optics scanning laser ophthalmoscopy (AOSLO) systems [7, 8]. These retinal imaging systems use a deformable mirror in combination with a wavefront sensor to correct for ocular aberrations and achieve cellular level imaging in the living eye [9, 10]. Fluorescence AOSLO has been used to demonstrate in vivo that the morphometry of retinal pigmented epithelial (RPE) cell mosaic varies considerably in the normal population and can be even more variable in diseased eyes [4, 9]. These measurements are obtained by segmentation and quantification of the morphometric properties of cells [11], such as cell area and density [7]. These quantitative metrics can then be used to evaluate cellular level alterations in disease [4] and to monitor disease progression. RPE cell metrics derived from cell segmentation can also be combined with photoreceptor topography measurements to quantify properties such as the number of photoreceptors per RPE cell. However, previous work using both short wavelength

[1]Department of Ophthalmology, University of Pittsburgh School of Medicine, Pittsburgh, PA, USA. [2]Department of Bioengineering, University of Pittsburgh Swanson School of Engineering, Pittsburgh, PA, USA. [3]McGowan Institute for Regenerative Medicine, University of Pittsburgh, Pittsburgh, PA, USA. [4]Present address: Department of Ophthalmology and Vision Science, University of California Davis, Sacramento, CA, USA. ✉email: kvienola@pitt.edu

excitation and AO-IRAF, showed that individual RPE cells can be difficult to segment no matter the method used, even in normal healthy eyes [7, 12], Thus, despite improvements to fluorescence AOSLO, there remains room for improvement to enable robust quantification of cells and to reduce the relatively long exposure times required for fluorescence AOSLO imaging or RPE cells.

As AO-IRAF capabilities have mostly been implemented into existing research systems, rather than systems designed specifically for AO-IRAF, the most often utilized excitation wavelength has been around 795 nm, a commonly chosen wavelength for infrared confocal reflectance imaging in AOSLO. Recently, Grieve et al. demonstrated that shifting to a slightly shorter wavelength of 757 nm for excitation [13], revealed the RPE mosaic in a similar way to previous research [4, 7, 14]. However, these experiments still required a relatively long exposure duration for the acquisition of each image.

Encouraged by the results from Grieve et al., showing AO-IRAF imaging of RPE with 757 nm excitation [13], and with the aim of determining an improved wavelength with increased efficiency for NIRAF, we set out to explore the possibility of imaging RPE structure with much shorter NIRAF excitation wavelengths, namely 663 nm, another commonly used wavelength in AOSLO. Melanin is thought to be the primary fluorophore contributing to the AO-IRAF signal, though recent evidence suggests that lipofuscin may also become excitable in the NIR with aging [15]. From the melanin absorption spectrum, it is evident that light absorption increases with shorter wavelengths. The absorption increases slightly with 757 nm excitation compared to 795 nm but with 663 nm, an almost threefold increase can be expected [5]. Absorption and excitation are usually correlated but whether the AF signal increases with shorter excitation wavelengths remains unknown and whether all the energy from shorter wavelength excitation is emitted as fluorescence.

To investigate the efficacy of using shorter wavelength excitation for NIRAF, we employed two different excitation beams, 663 nm, and 795 nm to excite the fluorophores in the RPE. NIRAF images were acquired sequentially with our AOSLO system that can record up to three channels simultaneously [12]. Our hypothesis was that the increased excitation light absorption would yield more AF signal. Because of this assumption, we kept the emission filter in the detection path the same for both excitation wavelengths despite the potential blue-shift in the AF peak when using the 663 nm excitation source.

METHODS
The details of the AOSLO system used in this study have been published previously [12]. In short, it utilizes three different light delivery channels for imaging (and excitation), namely 532 nm, 663 nm, and 795 nm. Signals from the retina (reflectance and/or fluorescence) are detected with three main channels, one channel being divided into two sub-channels for confocal reflectance and off-set imaging [16]. The pinhole size for confocal detection channels were 1 Airy disk diameter (ADD) for 795 nm and 1.1 for 663 nm. For the AF channel, a larger pinhole was used (1.8 ADD). The adaptive optics subsystem uses a 909 nm laser diode beacon to detect the aberrations and correct them in closed-loop mode that was separated from the data acquisition itself. Imaging data was acquired at 30 Hz recording always at least two channels simultaneously. One channel was always confocal reflectance, permitting eye motion to be tracked using strip-based motion correction [17] and applied to co-register the AO-IRAF frames [4], due to weak AF signal in individual frames. Images were registered with custom strip-based image registration and eye motion measurement software that is described in detail elsewhere [18]. This approach allows the motion of nearly all frames (~99% after excluding blink frames) to be detected with high spatial and temporal resolution. Strip-based fixational eye motion traces were computed using 16 strips per image frame (32 pixels high by 512 pixels wide). This type of image-based motion extraction allows much higher temporal sampling than permitted by the slow frame rate of the imaging system; these strip parameters yield eye traces at a nominal sampling frequency of 480 Hz.

The video recording length was empirically tested and varied between 60 and 90 s depending on the AF signal strength but was kept constant for each imaging session. To find an optimal pinhole location for the detector, a Nelder–Mead algorithm was used in conjunction with a motorized xyz-stage, as described previously [4]. To prevent excitation light leaking to the AF channel, double-stacked bandpass filters were used in front of the detector (FF01-832/37, Semrock, Rochester NY, USA) and 795 nm excitation source (ET775/50x, Chroma, Bellows Falls VT, USA). The time-averaged optical powers at the pupil plane were measured to be 50 µW (663 nm), 200 µW (795 nm), and 23 µW (909 nm). To ensure safe imaging, the ANSI laser safety limits were calculated using the latest standard [19]. Since all the wavelengths used in this study were above 600 nm, only thermal damage maximum permissible exposure (MPE) limits need to be calculated.

All volunteers were recruited through the research registry of the Clinical and Translational Science Institute of the University of Pittsburgh. Written informed consent was obtained from all participants following an explanation of experimental procedures and risks both verbally and in writing. All experiments were approved by the University of Pittsburgh Institutional Review Board and adhered to the tenets of the Declaration of Helsinki.

After the study participant was aligned in the system and AO correction was achieved, $1.5° \times 1.5°$ images were acquired starting with a 3 by 3 grid, with 50% overlap between adjacent fields, centred at fovea and then moving toward temporal regions, typically with a 1° step size. If the AO correction was subpar during imaging or patient was blinking a lot, image was reacquired from the same location. Otherwise, each location was imaged once with each wavelength.

Besides experimental AOSLO imaging, confocal reflectance (785 nm) imaging was done with commercial SLO system (Spectralis, Heidelberg, Germany). In addition, the subjects were imaged with a flood-illumination adaptive optics (FIAO) retinal camera (rtx1-e, ImagineEyes, Orsay, France), which provided $4° \times 4°$ high-resolution images of the photoreceptor mosaic using 850 nm illumination.

The signal-to-noise ratio (SNR) was quantified, using the following equation:

$$SNR = \frac{\mu_{sig} - \mu_{bg}}{\sigma_{sig}},$$

where μ_{sig} is the mean intensity value of the area containing the AO-IRAF signal, μ_{bg} the mean intensity of the vessel area that is defined as the background and σ_{sig} is the standard deviation of the AO-IRAF signal intensity. Furthermore, Michelson contrast was calculated with the following equation:

$$C = \frac{\mu_{sig} - \mu_{bg}}{\mu_{sig} + \mu_{bg}}.$$

RESULTS
Figure 1 shows example data of a healthy volunteer. Fig. 1(a) was acquired with a commercial SLO system. The red square indicates the area imaged with the FIAO retinal camera that is shown in Fig. 1(b). The FIAO image was taken 8° temporal from the fovea with image size of $4° \times 4°$. The expected cone mosaic is seen throughout the FOV and it corresponds with known healthy retina. The yellow square marks the area where the AOSLO images were taken using a 1.5° FOV (approximately at the same eccentricity as the FIAO). The middle row shows the averaged confocal reflectance images using 663 nm [Fig. 1(c)] and 795 nm [Fig. 1 (d)] laser sources, respectively. Both images show the expected cone mosaic for a healthy retina. Reflectance image with 663 nm is sharper compared to 795 nm due to the slight resolution advantage afforded by the shorter wavelength, and a smaller ADD resulting in a thinner depth sectioning and better out-of-focus light rejection. In addition, the 795 nm confocal image was acquired with a reflective pinhole [12], slightly decreasing the throughput and increasing the overall background noise compared to a true pinhole. The bottom row shows the AO-IRAF channel for both sources [Fig.1(e) & (f)]. The expected RPE cell mosaic structure is visible with both excitation wavelengths. No
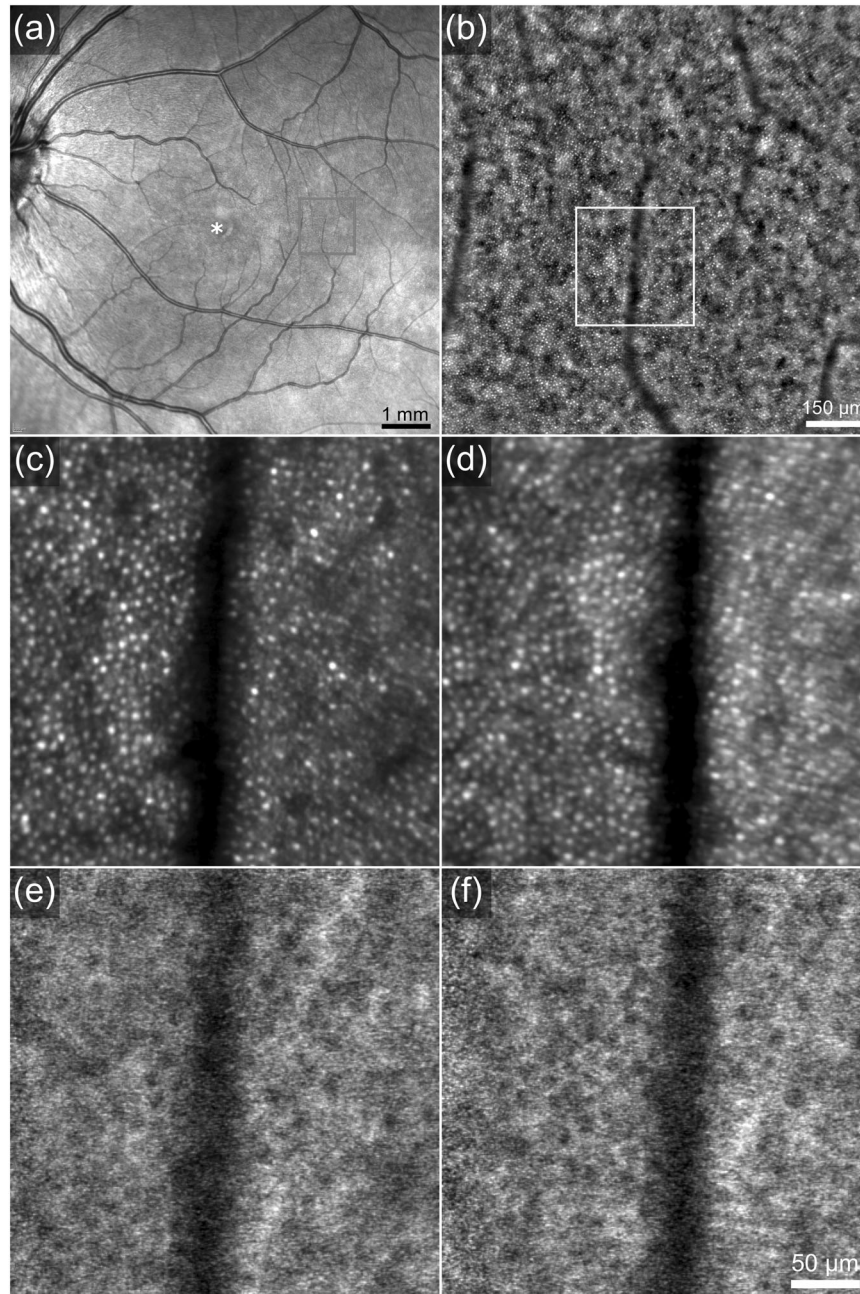
Fig. 1 AOSLO and NIRAF data from a healthy volunteer. a An SLO image showing the fovea marked with asterisk and red square indicating the area imaged with flood-illumination adaptive optics retinal camera (**b**) A 4°×4° retinal patch imaged with an FIAO retinal camera (8° temporal from fovea) showing the typical cone mosaic of a healthy person, yellow square indicates area imaged with AOSLO. **c** & **d** Confocal AOSLO reflectance images obtained with either 663 nm (**c**) or 795 nm (**d**) light. Resolution is slightly better in (**c**) due to the shorter wavelength and smaller confocal pinhole. **e** & **f** The averaged AOSLO NIRAF images. Both excitation wavelengths, 663 nm in (**e**) and 795 nm in (**f**), were able to produce similar AF structure of individual RPE cells, demonstrating the possibility of 663 nm excitation in NIRAF imaging. The fovea is marked with the asterisk.

distinct signal strength difference was noted when comparing the two AO-IRAF images. Both images showed microstructure and individual RPE cells. The SNR for the 663 nm excited AO-IRAF image was 1.71 [Fig. 1(e)] and 2.00 for 795 nm excitation [Fig. 1(f)]. Same trend was observed with the Michelson contrast, with 663 nm resulting at 0.35 and 0.40 for 795 nm.

Figure 2 shows data from a 67-year-old patient with degenerative maculopathy consistent with pattern dystrophy [20]. Infrared AF imaging (820 nm excitation) by SLO shows foci of both hyper- and hypoautofluorescence, and a geographic area of hypoautofluorescence [Fig. 2(a)]. The OCT B-scan [Fig. 2

(b)] shows, in this area, atrophy of the RPE and outer retina and, temporally, the location imaged by AOSLO (~6° temporal). On AOSLO, the typical RPE mosaic is not visualized (Fig. 2(d) and (f)), as is common when imaging patients with intermediate to advanced diseases [12]. The AO-IRAF image with 795 nm excitation shows areas that may be interpreted as enlarged RPE cells (Fig. 2(f), white arrows). The same structure is also seen in the AO-IRAF image excited with 663 nm exactly in the same location (Fig. 2(d), white arrows). Both AO-IRAF images reveal detailed microstructural alterations to the arrangement of the AF fluorophores. The round areas with decreased cone
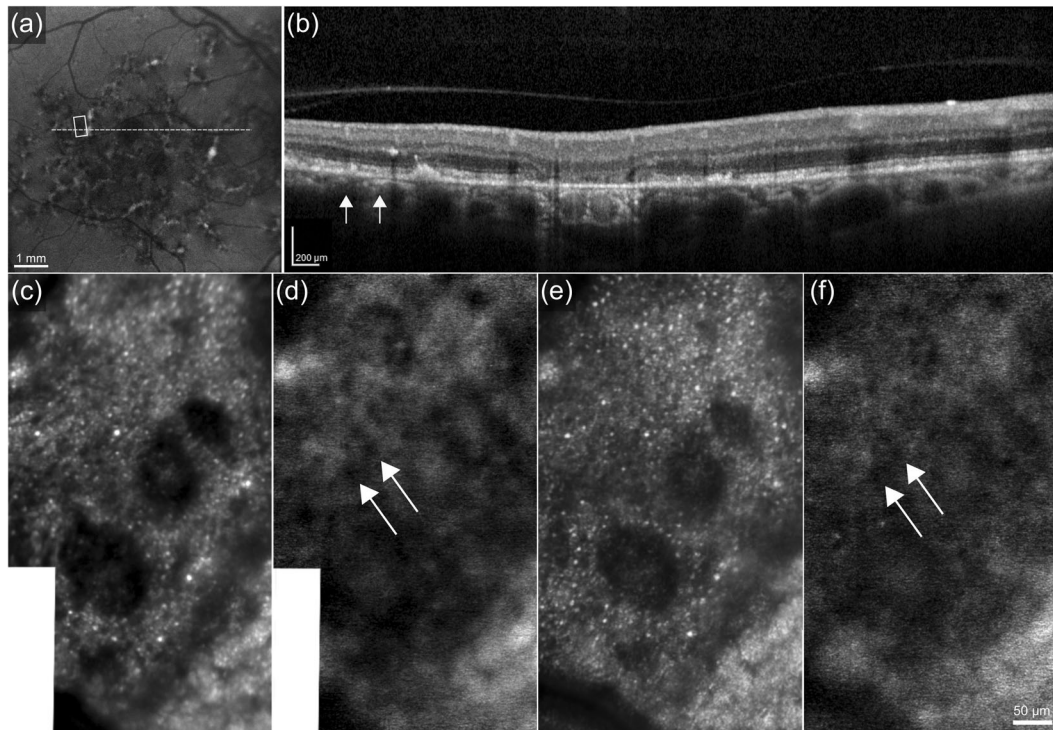
Fig. 2 Infrared autofluorescence (IRAF) and near-infrared autofluorescence (NIRAF) imaging of the right eye of a patient with degenerative maculopathy (~6° deg. eccentricity toward temporal region). a Infrared autofluorescence image from the right eye; yellow frame indicates position of AOSLO images; green line shows optical coherence tomography (OCT) scan line position. **b** Spectral domain OCT shows an area of hypertransmission, with retinal pigment epithelial (RPE) and outer retinal atrophy; subretinal hyperreflective material is seen temporally which is hyperautofluorescent in (**a**); yellow arrows indicate AOSLO image boundaries. **c** & **d** Reflectance and NIRAF images, respectively, taken with a 663 nm excitation source. **e** & **f** The same area imaged with a 795 nm source. The AF signal is weak but the upper part of both NIRAF images contains features that appear to be individual RPE cells (white arrows). The larger dark round areas salient in the confocal reflectance images are not seen in the NIRAF images.

Table 1. Summary of the obtained signal-to-noise ratio (SNR) values, contrast values and differences between the two wavelengths from seven different subjects.

Type	TIME [s]	SNR [dB]		Difference [%]	Michelson Contrast		Difference [%]
		663 nm	795 nm		663 nm	795 nm	
Control	75	2.13	1.98	+7.30	0.49	0.40	+20.22
Control	75	1.97	1.79	+9.57	0.49	0.48	2.06
Patient	75	2.13	1.44	+38.66	0.43	0.41	4.76
Patient	75	3.16	2.81	+11.73	0.56	0.60	−6.90
Patient	75	1.04	1.00	3.92	0.21	0.30	−35.29
Patient	90	1.72	1.48	+15.00	0.53	0.45	+16.33
Control	75	1.71	2.00	−15.63	0.35	0.40	−13.33

reflectivity, potentially due to cone outer segment alterations or cone loss, salient in the reflectance images, do not appear to manifest in any way in the AO-IRAF images. The confocal channel (both 663 nm and 795 nm) visualizes the photoreceptors well, as the small ADD of the confocal pinhole eliminates light scattered from out-of-focus layers efficiently, resulting in sharper contrast. With both excitation wavelengths the AO-IRAF signal is mostly nonuniform and shows microstructures that do not correspond to the structures in the confocal channel. For the 663 nm and 795 nm excitation light the

resulting SNRs were 1.72 and 1.48, respectively. The Michelson contrast was similar between both wavelengths, 0.53 for 663 nm and 0.45 for 795 nm.

Table 1 shows SNR and contrast data from additional five subjects (two healthy and three patient) using 663 nm and 795 nm excitation wavelengths. There is ~10–15% difference between the SNR and contrast values overall. This similar trend is also seen in Fig. 3, where the mean SNR and Michelson contrast are plotted for each wavelength and for both groups. The SNR values showed no meaningful difference between 663 nm and 795 nm excitation
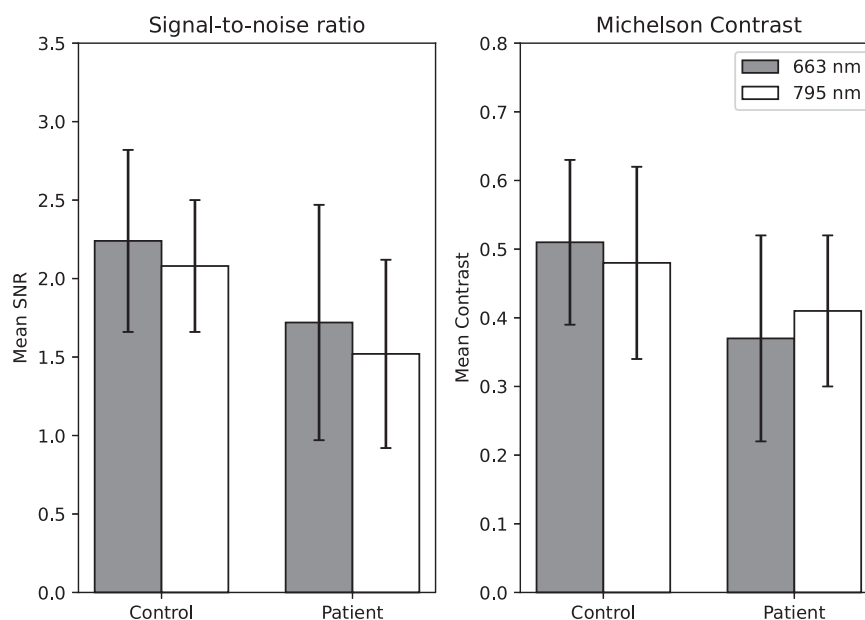
Fig. 3 Signal-to-noise ratio and Michelson contrast were similar for each excitation wavelength. SNR values were slightly higher with 663 nm excitation. There was only a small difference in the contrast between the two excitation wavelengths with 795 nm excitation producing slightly better contrast in the patient group. Overall, the contrast and SNR were better (as expected) in the control group compared to the patient group, regardless of the excitation wavelength. The error bars are ± one standard deviation.

and similar trend was observed in the contrast between the two excitation wavelengths.

DISCUSSION
Individual RPE cells and AO-IRAF fluorophore microstructure can be visualized using even shorter wavelengths than previously utilized [7, 13, 14], suggesting that fluorophores that emit within the NIR are broadly excitable, down to at least the wavelength tested here. We observed comparable structure in the AO-IRAF images obtained with 663 nm excitation even though we used around four times lower excitation power at 663 nm. Whether this excitation wavelength is exciting different fluorescent organelles than those that are excited with 795 nm requires further study, but we see extensive co-localized fluorescence in the few eyes we have examined. Recently, Taubitz et al. showed that lipofuscin starts out as being autofluorescent only with short-wavelength excitation but becomes excitable with NIR light with age. Their hypothesis was that lipofuscin incorporates melanin oxidation products over time into its complex granule structure [15]. How age and disease alter the abundance, composition, and spectra of the fluorophores responsible for NIRAF warrants further study.

Several additional aspects are still to be considered. Firstly, there is uncertainty about how AF signal strength is reduced when the same area is imaged twice with two different excitation beams. The 663 nm excitation was used after 795 nm in Fig. 2, but no qualitative loss of AF signal is observed, which is also then confirmed by the SNR and contrast calculations. It was shown previously that NIRAF signal can decrease with extended NIRAF exposures, just like SWAF, but that the NIRAF signal recovers over much longer timescales [21]. However, we found that we were able to reliably image the same cells in some eyes at several time points, suggesting that the signal reduction is modest. It did not interfere with repeated measurements nor there was a clear-cut difference in signal between previously exposed regions and the next one when acquiring data [12]. The emission window, as mentioned, was kept the same for both excitation sources as we wanted to evaluate whether it was feasible to achieve emission in the same band, potentially of the same fluorophores. Blue-shifting and broadening the emission window could both contribute to increased signal

strength. Another aspect that may influence the signal is the smaller excitation volume as the axial point-spread function is smaller with 663 nm than 795 nm Finally, even though the focal planes were carefully aligned to be the same, it is likely that there was some difference in focal plane between the two sources, with different fluorophores excited, however we do not anticipate that excitation volume would be substantially different axially in each case.

Due to spectral sensitivity differences of the eye, the 663 nm light appeared brighter to the subject than the 795 nm excitation light despite the higher power levels used for 795 nm excitation compared to 663 nm. When considering the addition of the 909 nm light used for the wavefront sensing beacon, each pair of wavelengths used simultaneously was below the ANSI limits. In fact, even if all three sources were used simultaneously, they would remain well below the ANSI safety guidelines. When considering safety for multiple light sources, the percentage of MPE for each different source is calculated and summed [22]. Considering these for this study the 663 nm can produce comparable AF signal with much smaller fractional MPE levels (13% for 663 nm vs. 34% for 795 nm). The more pleasant viewing experience for 795 nm allows more power to be used with no discomfort to the patient but it also bypasses the nature's own safety mechanism, the blink reflex. The contribution of the 909 nm light is negligible in this scenario as the 23 µW only contributes 0.023 to the total sum of the MPE fractions.

In summary, we have shown here our first results from our experimental AO-IRAF imaging using 663 nm and 795 nm excitation light to image the structure of the RPE cell layer. The images show very similar microstructure, especially with the healthy volunteer. The patient with maculopathy exhibits structure in the AO-IRAF images that is consistent with our previous results obtained in patients with AMD, when imaging AO-IRAF using 795 nm excitation [12]. Results with 663 nm excitation demonstrate the feasibility of using even shorter wavelengths to excite AO-IRAF fluorophores. Further investigation is needed to define the AF profile of the macula across the visible and into the NIR, and to determine how this AF changes with aging and in disease. Understanding these changes with age and disease is essential for the development of improved diagnostic tools to assess macular health through AF imaging.

SUMMARY

What was known before

- The retinal pigmented epithelium (RPE) contains fluorophores that can be excited with visible and near-infrared wavelengths of light and AF imaging of the RPE is important for studying and monitoring diseases of the outer retina, such as AMD The excitation and emission bands of RPE fluorophores may shift in aging and disease RPE AF can be used in adaptive optics ophthalmoscopy to visualize the cellular structure of the RPE in vivo.
- Near-infrared AF using adaptive optics assisted ophthalmoscopy (AOO) has succesfully imaged RPE cells with excitation wavelengths as short as 757 nm, but the efficacy of shorter wavelengths has not been evaluated.

What this study adds

- RPE cells can be imaged using NIRAF in AOO with excitation wavelengths as short as 663 nm, expanding the useful range for NIRAF excitation into the visible.
- Though the images are qualitatively similar, some differences exist in the appearance of RPE cells when imaged with different excitation wavelengths.

REFERENCES

1. Delori FC. Spectrophotometer for noninvasive measurement of intrinsic fluorescence and reflectance of the ocular fundus. Appl Opt. 1994;33:7439–52.
2. Delori FC, Dorey CK, Staurenghi G, Arend O, Goger DG, Weiter JJ. In vivo fluorescence of the ocular fundus exhibits retinal pigment epithelium lipofuscin characteristics. Investig Ophthalmol Vis Sci. 1995;36:718–29.
3. von Rückmann A, Fitzke FW, Bird AC. Fundus autofluorescence in age-related macular disease imaged with a laser scanning ophthalmoscope. Investig Ophthalmol Vis Sci. 1997;38:478–86.
4. Rossi EA, Rangel-Fonseca P, Parkins K, Fischer W, Latchney LR, Folwell MA, et al. In vivo imaging of retinal pigment epithelium cells in age related macular degeneration. Biomed Opt Express. 2013;4:2527–39.
5. Keilhauer CN, Delori FC. Near-infrared autofluorescence imaging of the fundus: visualization of ocular melanin. Investig Ophthalmol Vis Sci. 2006;47:3556–64.
6. Morgan JIW, Dubra A, Wolfe R, Merigan WH, Williams DR. In Vivo Autofluorescence Imaging of the Human and Macaque Retinal Pigment Epithelial Cell Mosaic. Investig Ophthalmol Vis Sci. 2009;50:1350–9.
7. Granger CE, Yang Q, Song H, Saito K, Nozato K, Latchney LR, et al. Human Retinal Pigment Epithelium: In Vivo Cell Morphometry, Multispectral Autofluorescence, and Relationship to Cone Mosaic. Investig Ophthalmol Vis Sci. 2018;59:5705–16.
8. Liu Z, Tam J, Saeedi O, Hammer DX. Trans-retinal cellular imaging with multimodal adaptive optics. Biomed Opt Express. 2018;9:4246–62.
9. Liang J, Williams DR, Miller DT. Supernormal vision and high-resolution retinal imaging through adaptive optics. J Opt Soc Am A 1997;14:2884–92.
10. Roorda A, Romero-Borja F, Donnelly WJ III, Queener H, Hebert TJ, Campbell MCW. Adaptive optics scanning laser ophthalmoscopy. Opt Express. 2002;10:405–12.
11. Rangel-Fonseca P, Gómez-Vieyra A, Malacara-Hernández D, Wilson MC, Williams DR, Rossi EA. Automated segmentation of retinal pigment epithelium cells in fluorescence adaptive optics images. J Opt Soc Am A 2013;30:2595–604.
12. Vienola KV, Zhang M, Snyder VC, Sahel J-A, Dansingani KK, Rossi EA. Microstructure of the retinal pigment epithelium near-infrared autofluorescence in healthy young eyes and in patients with AMD. Sci Rep. 2020;10:9561.
13. Grieve K, Gofas-Salas E, Ferguson RD, Sahel JA, Paques M, Rossi EA. In vivo near-infrared autofluorescence imaging of retinal pigment epithelial cells with 757 nm excitation. Biomed Opt Express. 2018;9:5946–61.
14. Liu T, Jung H, Liu J, Droettboom M, Tam J. Noninvasive near infrared autofluorescence imaging of retinal pigment epithelial cells in the human retina using adaptive optics. Biomed Opt Express. 2017;8:4348–60.
15. Taubitz T, Fang Y, Biesemeier A, Julien-Schraermeyer S, Schraermeyer U. Age, lipofuscin and melanin oxidation affect fundus near-infrared autofluorescence. EBioMedicine . 2019;48:592–604.
16. Rossi EA, Granger CE, Sharma R, Yang Q, Saito K, Schwarz C, et al. Imaging individual neurons in the retinal ganglion cell layer of the living eye. Proc Nat Acad Sci USA. 2017;114:586–91.
17. Arathorn DW, Yang Q, Vogel CR, Zhang Y, Tiruveedhula P, Roorda A. Retinally stabilized cone-targeted stimulus delivery. Opt Express. 2007; 15:13731.
18. Zhang M, Gofas-Salas E, Leonard BT, Rui Y, Snyder VC, Reecher HM, et al. Strip-based digital image registration for distortion minimization and robust eye motion measurement from scanned ophthalmic imaging systems. Biomed Opt Express. 2021;12:2353–72.
19. Laser Institute of America. American National Standard for Safe Use of Lasers. ANSI Z1361-2014.
20. Marmor MF, Byers B. Pattern Dystrophy of the Pigment Epithelium. Am J Ophthalmol. 1977;84:32–44.
21. Masella BD, Williams DR, Fischer WS, Rossi EA, Hunter JJ. Long-Term Reduction in Infrared Autofluorescence Caused by Infrared Light Below the Maximum Permissible Exposure. Investig Ophthalmol Vis Sci. 2014;55:3929–38.
22. Lyon T. Hazard analysis technique for multiple wavelength lasers. Health Phys. 1985;49:221–6.

AUTHOR CONTRIBUTIONS

EAR and JAS conceived the experiments, KVV and EAR conducted the experiment(s), EAR, KKD and KVV analyzed the results. VCS conducted the clinical imaging. MZ developed the custom electronics and control software. KVV wrote the paper, EAR edited the paper, and all other co-authors carefully reviewed the paper for scientific content.

Funding

COMPETING INTERESTS

Some aspects of this work include technologies that Dr EAR is an inventor on for patents that are owned by the University of Rochester (US Patent No.: US 10,123,697 and US 10,092,181). Dr KKD is a consultant for Biogen. No other authors have any competing interests related to this work.

ADDITIONAL INFORMATION

Correspondence and requests for materials should be addressed to K.V.V.

Reprints and permission information is available at http://www.nature.com/reprints

Publisher's note Springer Nature remains neutral with regard to jurisdictional claims in published maps and institutional affiliations.